Journal of Sound and Vibration (2001) **239**(3), 379–396
doi:10.1006/jsvi.2000.3173, available online at http://www.idealibrary.com on IDEAL®

A TIME-DOMAIN METHOD FOR THE PREDICTION OF SOUND ATTENUATION IN LINED DUCTS

L. SBARDELLA

Department of Mechanical Engineering, Imperial College of Science, Technology and Medicine, London SW7 2BX, U.K. E-mail: l.sbardella@ic.ac.uk

B. J. TESTER

Rolls-Royce, P.O. Box 31, Derby DE 24 8BJ, U.K.

AND

M. IMREGUN

Department of Mechanical Engineering, Imperial College of Science, Technology and Medicine, London SW7 2BX, U.K. E-mail: m.imregun@ic.ac.uk

(*Received* 8 *December* 1998, *and in final form* 10 *April* 2000)

This paper describes the development and application of a time-domain acoustic liner model which is suitable for the simulation of sound propagation and attenuation in lined ducts. The fluid flow within the duct domain is represented by the non-linear, unsteady Euler equations while the liner model consists of a resistive frequency-independent part and a reactive part which is obtained by solving the one-dimensional Euler equations within the liner cavity. Specialized boundary conditions are used for matching the 1D cavity flow and the 2D duct flow. The liner model has been formulated in order to predict the sound attenuation with or without mean flow, as well as for linear or non-linear sound propagation. The model has been validated in the case of linear pure-tone and *N*-wave signals by checking against analytical formulations obtained via eigensolutions of the linearized inviscid flow equations. Very good agreement was obtained for both zero and subsonic mean flows.

1. INTRODUCTION

As the bypass ratio is increased, the level of noise emitted from the inlet of modern turbofan engines is becoming a significant component of the overall aircraft noise levels. Aero-engine manufacturers are therefore aiming at reducing the level of noise emitted from the inlet of turbofan-engines, especially during landing and take-off. Current engine designs treat nacelle inlets with laminar liners composed of porous sheets with backing air cavities. It is highly desirable to be able to predict the liner efficiency for various speed conditions and hence an accurate mathematical model of the liner needs to be developed. Accordingly, the aim of this work is to formulate a numerical model for the time-domain simulation of duct acoustics in the presence of sound-absorbing liners.

Myers [1] derived a general acoustic impedance boundary condition by assuming that a soft wall, i.e., an acoustically treated surface, undergoes a deformation in response to an

0022-460X/01/030379 + 18 $35.00/0

incident acoustic field from the fluid. He also assumed that these deformations were small perturbations to a stationary mean surface, and that the corresponding fluid velocity field was a small perturbation about a steady non-linear mean flow. Such a frequency-domain impedance condition can be expressed as:

$$\hat{\mathbf{v}} \cdot \mathbf{n} = -\frac{\hat{p}}{\mathscr{Z}} - \frac{1}{\mathrm{i}\omega} \bar{\mathbf{v}} \cdot \nabla \left(\frac{\hat{p}}{\mathscr{Z}} \right) + \frac{\hat{p}}{\mathrm{i}\omega \mathscr{Z}} \mathbf{n} \cdot (n \nabla \cdot \bar{\mathbf{v}}), \tag{1}$$

where $\hat{\mathbf{v}}$ and $\hat{p}$ are the complex amplitudes of the velocity and pressure perturbations, ω is the circular frequency, $\mathbf{n}$ is the mean surface normal pointing away from the surface, $\bar{\mathbf{v}}$ is the mean velocity about which the linearization is performed and $\mathscr{Z}$ is the impedance. A harmonic time variation of the form $\exp(\mathrm{i}\omega t)$ is implicitly assumed. The impedance can be expressed as [2]:

$$\mathscr{Z}(\omega) = \overline{\rho c} [\mathscr{R}(\omega) + \mathrm{i}\mathscr{X}(\omega)], \tag{2}$$

where $\mathscr{R}(\omega)$ and $\mathscr{X}(\omega)$ are the frequency-dependent specific acoustic resistance and reactance. $\bar{\rho}$ and $\bar{c}$ are the mean fluid density and speed of sound.

To the authors' knowledge, very few time-domain simulations of duct acoustics with soft walls exist in the open literature. A time-domain implementation of the Myers impedance boundary condition [1] was used in reference [3] to study the liner effects. An inverse Fourier transform of equation (1) is needed in order to use the Myers formulation in the time domain. As stated in reference [3], such an inverse Fourier transform results in a convolution equation which is computationally expensive, low in accuracy and hence impractical for multi-dimensional computational aeroacoustic problems. In reference [3], this problem is overcome by using a z-transform and the impedance is expressed as a ratio of two polynomial functions of frequency. The main drawback of such an approach is the need to calibrate the polynomial functions for the specific conditions of the case under study.

A different time-domain approach for simulating liners composed of porous sheets with backing air cavities was given by Reichert and Biringen [4]. The liner is modelled as a continuous empirical source term which modifies the right-hand side of the inviscid flow momentum equations. The time-domain behaviour of the frequency-domain resistance and reactance of the liner's porous sheets are specified through this source term. Therefore, the liner effect is seen to be interior to the domain rather than through finite impedance boundary conditions as in reference [3]. The source term contains four empirical parameters which specify the levels of linear and non-linear resistance as well as the linear reactance of each porous sheet in the time domain. These parameters are matched to frequency-domain impedance data via a numerical simulation of a one-dimensional impedance tube.

The classical Myers impedance condition was derived by assuming small pressure perturbations and linear behaviour. The more general treatment of Reichert and Biringen [4], that can deal with the non-linear behaviour of the liner at high sound–pressure levels, is too expensive for realistic 3D geometries such as fan assembly plus intake duct. A practical liner model must be as simple as possible without any explicit frequency dependence since the aim is to incorporate it into large CFD calculations of fan assemblies with intake ducts. Such a task is achieved by treating the duct and the liner backing air cavity as two different domains which interact with each other through novel boundary conditions simulating the presence of the liner porous sheets. Non-linear unsteady Euler equations are used to model both the duct domain and the liner cavities, though 2D flow is assumed for the former and

1D flow for the latter. As such, the time-domain liner model proposed here can be considered to be a simplification of that proposed by Reichert and Biringen. As will be discussed in section 3.2, a velocity discontinuity arises between the duct and the liner domains for inviscid main duct flows. A solution is to apply linearized boundary conditions at the discontinuity but such a liner modelling route is not necessarily beneficial over the Myers impedance condition. However, if the flow in the liner is of some interest, or if there is a requirement to rank the performance of several types, the 1D Euler modelling of the liner may be advantageous. Furthermore, the velocity discontinuity will no longer exist if the duct flow can be modelled in a viscous fashion with the no-slip condition and hence the proposed methodology will become more attractive.

2. GOVERNING EQUATIONS

The unsteady flow field in the duct is modelled by the 2D Euler equations, the conservation form of which can be written as:

$$\frac{\partial \mathbf{U}}{\partial t} + \frac{\partial \mathbf{F}}{\partial x} + \frac{\partial \mathbf{G}}{\partial y} = 0. \tag{3}$$

The solution vector of conservative variables $\mathbf{U}$ is given by:

$$\mathbf{U} = \begin{bmatrix} \rho \\ \rho u \\ \rho v \\ \rho E \end{bmatrix}. \tag{4}$$

The inviscid flux vectors $\mathbf{F}$ and $\mathbf{G}$ have the following forms:

$$\mathbf{F} = \begin{bmatrix} \rho u \\ \rho u^2 + p \\ \rho uv \\ \rho Hu \end{bmatrix}, \qquad \mathbf{G} = \begin{bmatrix} \rho v \\ \rho vu \\ \rho v^2 + p \\ \rho Hv \end{bmatrix}, \tag{5, 6}$$

The pressure p and the total enthalpy H are related to the density ρ, the velocity components u and v and the total energy E by two perfect gas equations:

$$p = (\gamma - 1)\rho\left[E - \frac{u^2 + v^2}{2}\right], \quad H = E + \frac{p}{\rho}, \tag{7}$$

where γ is a constant specific heats ratio. The local speed of sound is given by:

$$c = \sqrt{\gamma \frac{p}{\rho}}. \tag{8}$$

The spatial discretization of equation (3) is obtained by using a central difference scheme with added matrix artificial dissipation [5, 6]. The time integration procedure, described by Shu [7], is an explicit three-stage Runge–Kutta scheme. Two-dimensional non-reflective boundary conditions are applied to the open boundaries in order to reduce the amount of numerical reflections of the outgoing waves [8].

3. LAMINAR LINER MODEL

Laminar liners have been widely used in aircraft turbo-fan ducts, owing to their potential for high mechanical integrity, and resistance to corrosive substances and erosion [9]. A laminar liner is composed of a relatively thin layer of porous material suspended over a cavity which terminates with a reflective backing sheet (see Figure 1). The thin layer of porous material, which represents the interface between the main duct domain and the backing air cavities, acts almost wholly as an acoustic resistance, while the cavities act almost wholly as an acoustic reactance [2]. Up to quite high frequencies, the laminar liner construction allows a particularly simple approximate expression for the calculation of its specific acoustic impedance in terms of the specific flow resistance, $\mathscr{R}$, of the porous surface layer and the depth, d, of the cavity [2]. Upon neglecting the inertia and stiffness of the micro-structure of the porous material matrix, the laminar liner impedance can be written as

$$\mathscr{Z}(\omega) = \overline{\rho c}\left[\mathscr{R}(\omega) + \mathrm{i}\cot\left(\frac{\omega d}{\bar{c}}\right)\right]. \tag{9}$$

3.1. TIME-DOMAIN RESISTANCE MODEL

The specific laminar liner resistance R has little effect upon the frequency of maximum attenuation but it governs the maximum attenuation achieved and the bandwidth of the attenuation [2]. Therefore, in engineering terms, $\mathscr{R}$ may be considered to be frequency-independent for many thin porous materials, a first assumption in the derivation of the liner model.

The acoustic resistance of a thin layer of a porous material can be approximated by its specific flow resistance, the ratio between the pressure difference across the material and the velocity of the flow through the material

$$\rho c R_t = \frac{p_d - p_l}{v_l}. \tag{10}$$

Here p_d and p_l are the pressure in the duct and in the liner cavity domains respectively. v_l is the flow velocity through the porous sheet material, the positive direction being from the main duct domain towards the liner cavity.

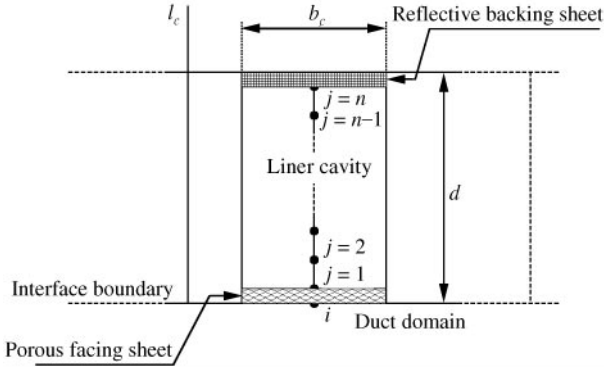

Figure 1. Liner model.

The liner resistance R_t is particularly sensitive to the sound–pressure level. The relationship between the sound–pressure level and the resistance can be modelled by using a non-linear approximation which takes into account the velocity v_l of the flow through the thin porous material,

$$R_t = R_l + R_n \left| \frac{v_l}{c} \right|, \tag{11}$$

where R_l and R_n are two known constants which depend upon the liner material.

Broadly speaking, the behaviour in the porous layer is somewhat difficult to gauge and hence it is not straightforward to assess when the non-linear term is going to be important. Depending on the level of the perturbations, i.e. sound–pressure levels, liners are likely to show a non-linear behaviour. Generally speaking, when the velocity through the liner increases, the liner resistance also increases and the attenuation drops. In any case, some very useful physical insight may be gained by considering specific cases[†]. For pores in the liner top layer that are small enough, the local Reynolds number will also be small. If the layer is much thinner than a wave length, the flow in the pore may be considered to be incompressible. For such Stokes flows, the velocity will be proportional to the pressure difference, as indicated by equation (10). If the local pore velocity becomes large, the Reynolds number will no longer be small and the relationship between the velocity and pressure differential will become non-linear. In particular, inertial effects leading to jet formation will make the relationship mean-flow dependent as the jets will interact with the mean flow. Such considerations help towards explaining why the material properties of the liner may give rise to significant non-linear effects. For instance, compared to porous layers and woven metal, perforated plate liners are both amplitude and mean-flow dependent because of the high-velocity and jet-formation effects.

As cited by Melling [9], the non-linear part of the acoustic impedance can dominate the acoustic behaviour of the material at sound–pressure levels of interest in aero-engine applications. For small perturbations, it is possible to ignore the non-linear term and such a route will be followed here when comparing numerical and analytical results for linear cases. If the non-linear effects are likely to be important, the non-linear part R_n should be included in the calculations. However, in this case, the main duct domain should be modelled via Navier–Stokes equations with the no-slip condition to ensure compatibility at the wall. This will be discussed now in more detail.

3.2. TREATMENT OF THE VELOCITY DISCONTINUITY ACROSS THE LINER

Equation (10), which assumes an instantaneous pressure jump across the porous sheet, is used to evaluate the normal velocity at a given duct/liner-cavity interface. For an inviscid computation, equation (10) is valid only when there is no mean flow in the duct, i.e., when there is no boundary layer. In the presence of a mean flow, the duct-domain velocity normal to the lined wall boundary, v_d, cannot be evaluated via equation (10) by using pressures computed for an inviscid flow. This limitation is due to the absence of the boundary layer effects which can play an important role in the sound attenuation process. In the area of duct acoustics, a great deal of discussion exists over the apparent differences in the condition depending upon whether the mean flow is treated as viscous or inviscid [1, 10, 11]. It is usually accepted that, when the base flow is treated as inviscid, the proper kinematic condition at a lined wall must be expressed physically by the requirement of

[†]The contribution of the referee is gratefully acknowledged.

continuity of acoustic particle displacement [1]. More specifically, such a requirement means that the displacement of a fluid particle in the direction normal to the lined-wall boundary must be equal to the displacement of the corresponding fluid particle in the liner. For a fluid particle moving parallel to the x-axis with a mean axial velocity $\bar{u}$, the particle displacement d_p and the normal velocity v are related by:

$$v = \frac{\mathrm{D}d_p}{Dt} = \frac{\partial d}{\partial t} + \bar{u}\frac{\partial d}{\partial x}. \tag{12}$$

Such a relationship is valid just above and just below the lined wall. Such a consideration yields:

$$v_l = \frac{\partial d}{\partial t}, \quad v_d = \frac{\partial d}{\partial t} + \bar{u}\frac{\partial d}{\partial x}, \tag{13, 14}$$

where v_l is the normal velocity of the particle just above the lined wall (i.e., in the liner cavity), and v_d is the normal velocity of the particle just below the lined wall (i.e., in the duct domain). Combining equations (13) and (14) and differentiating with respect to time, one obtains a relationship between the two normal velocities:

$$\frac{\partial v}{\partial t} = \frac{\partial v}{\partial t} + \bar{u}\frac{\partial v}{\partial x}. \tag{15}$$

Equation (15) shows that there is a discontinuity of normal velocity across the vortex sheet in the case of non-zero mean flow. This jump condition is applied at the stationary lined wall by linearizing equation (15) around $y = 0$. Such a route is very much analogous to the classical Myers impedance boundary condition. However, the approximate linearized treatment can be avoided by using Navier–Stokes modelling with the no-slip condition. Such an approach will remove the discontinuity by ensuring that $v_l = v_d$ and the non-linear effects will be included.

3.3. DUCT-CAVITY BOUNDARY CONDITIONS

The cavity depth d has little effect on the peak attenuation and attenuation bandwidth, but it strongly influences the tuned frequency of the liner [2]. Since the width of the liner cavity is usually very small compared to its length, it is reasonable to assume that only plane waves will propagate within the cavity. If the viscous effects can be neglected, the 1D Euler equations should, in principle, be adequate to model the flow within the liner cavity, both for linear and non-linear flow regimes. Although 3D effects may occur near the exit, these are likely to be small for slender cells. In any case, a 1D liner model will be adopted here for the numerical studies.

The computational domain for a typical liner cavity is shown in Figure 1, where n denotes the number of points used to discretize the cavity depth. At the reflective backing sheet ($j = n$), the velocity is set to zero during the time evolution while the pressure is extrapolated from the interior domain. At the porous sheet ($j = 1$), special boundary conditions, that will be described below, are applied in order to match the value of the velocity v_l obtained from the liner resistance model.

It is well known that the treatment of boundary conditions is extremely important for Euler equations and the chosen scheme can have a significant effect on the solution. Such a strong influence stems from the physical nature of the convection or propagation

phenomena [12]. The number of physical variables that can be imposed freely at a boundary is dependent on the propagation properties of the system and, in particular, on the information propagated from the boundary towards the inside of the flow region. In order to illustrate the boundary conditions adopted in the duct-liner cavity interface, one can re-write the 1D Euler equations at this interface in a diagonalized form,

$$\frac{\partial}{\partial t}\begin{bmatrix} w_1 \\ w_2 \\ w_3 \end{bmatrix} + \begin{bmatrix} v_l & 0 & 0 \\ 0 & v_l + c & 0 \\ 0 & 0 & v_l - c \end{bmatrix} \frac{\partial}{\partial x}\begin{bmatrix} w_1 \\ w_2 \\ w_3 \end{bmatrix} = 0, \tag{16}$$

where

$$\begin{bmatrix} \delta w_1 \\ \delta w_2 \\ \delta w_3 \end{bmatrix} = \begin{bmatrix} -c^2 & 0 & 1 \\ 0 & \rho c & 1 \\ 0 & -\rho c & 1 \end{bmatrix} \begin{bmatrix} \delta\rho \\ \delta v \\ \delta p \end{bmatrix}. \tag{17}$$

The characteristic form of the Euler equation is thus given by equation (16) and the quantities δw_i represent the characteristic variables. Such variables are associated with plane waves; in particular δw_1 is the entropy wave with speed u, δw_2 is the forward acoustic wave with speed $u + c$ and δw_3 is the backward acoustic wave with speed $u - c$. When the flow is propagating from the duct domain into the liner cavity ($v_l > 0$), there will be two characteristic variables which propagate from the duct domain into the liner cavity, i.e., δw_1 and δw_2 because of their subsonic convection speed ($v_l < c$). On the other hand, if the flow originates from the cavity ($v_l < 0$), only one characteristic variable, δw_2, will be propagating towards the cavity domain.

Following from these considerations, there are two cases for dealing with the boundary conditions at $j = 1$ in Figure 1: two boundary conditions are required if $v_l > 0$ and only one boundary condition only if $v_l \leqslant 0$. However, the only available physical quantity that can be imposed is v_l. Thus, an extra numerical boundary condition is needed for the case of $v_l > 0$. This extra boundary condition is obtained by setting the first characteristic variable to zero, which means that there is no entropy wave propagating towards the liner domain.

4. NUMERICAL IMPLEMENTATION

The numerical implementation of the liner model of section 3 will be presented here. First, the discretization of the resistance model is discussed in some detail since it plays an important role for an accurate numerical prediction of the sound attenuation.

4.1. LINER RESISTANCE MODEL

The liner resistance model is represented by three equations, namely equations (10), (11), and (15). Before going into the details of the numerical scheme, it is worth identifying the input and the output variables. In the following equations, the superscript m indicates a time instant $t^m = t^0 + m\Delta t$, where Δt is the time step for the numerical integration. With reference to Figure 1, the input variables are (i) $p_l^m = p_{j=1}^m$ in equation (10), (ii) $p_d^m = p_i^m$; also in equation (10)† and (iii) v_l^m. The output variables are v_l^{m+1} and v_d^{m+1}.

†i is the point corresponding to $j = 1$ in the duct domain.

The numerical algorithm for the liner resistance is implemented at the beginning of the new time step, which advances the overall solution from time t^m to time t^{m+1}. The time discretization of equation (15) leads to the following numerical approximation:

$$\frac{\Delta(v_l - v_d)_i^{m+1}}{\Delta t} + \bar{u}\frac{\partial v_l^{m+1}}{\partial x} = 0. \tag{18}$$

In order to guarantee the numerical stability of equation (18), the convective space derivative is implemented by using a first order upwind algorithm. The numerical implementation of equation (18) on an equi-spaced 1D grid takes the form:

$$\frac{\Delta(v_l - v_d)_i^{m+1}}{\Delta t} + \frac{\bar{u}}{2\Delta x}(v_{l_{i+1}} - v_{l_{i-1}})^{m+1} - \frac{|\bar{u}|}{2\Delta x}(v_{l_{i+1}} - 2v_{l_i} + v_{l_{i-1}})^{m+1} = 0. \tag{19}$$

By using such a first order formulation, problems related to undamped numerical errors are avoided. The numerical implementation of the liner resistance model can be summarized as:

$$R_{td_i}^{m+1} = R_l + R_{nl}\left|\frac{v_{l_i}^m}{c}\right|, \quad v_{l_i}^{m+1} = \frac{p_i^m - p_{j=1}^m}{\rho c R_{td_i}^{m+1}}, \tag{20, 21}$$

and v_d^{m+1} is obtained from equations (19) and (21).

4.2. LINER CAVITY MODEL

The liner reactance model is based on the numerical solution of the 1D Euler equations on an equi-spaced mesh within the liner cavity and the numerical algorithm is similar to that employed in the duct domain. The two domains are coupled together by matching the liner velocity v_l^{m+1} at $j = 1$ (see Figure 1) and the normal velocity v_d^{m+1} in the duct wall domain. With the change in the primitive variables due to the interior algorithm indicated with subscript *int*, the boundary treatment becomes as follows.

Case $v_l^{m+1} > 0$. The changes in the characteristic variables are given by:

$$\delta w_1 = 0, \quad \delta w_2 = \rho c(v_l^{m+1} - v_l^m), \quad \delta w_3 = \delta p_{int}. \tag{22–24}$$

Inverting equation (17) yields:

$$\delta\rho^{m+1} = \frac{1}{2c^2}[\rho c(v_l^{m+1} - v_l^m) + \delta p_{int}], \quad \delta v^{m+1} = v_l^{m+1} - v_l^m, \quad \delta p^{m+1} = c^2\delta\rho^{m+1}. \tag{25–27}$$

Case $v_l^{m+1} < 0$. The changes in the characteristic variables are given by:

$$\delta w_1 = \delta p_{int} - c^2\delta\rho_{int}, \quad \delta w_2 = \rho c(v_l^{m+1} - v_l^m), \quad \delta w_3 = \delta p_{int}. \tag{28–30}$$

Inverting equation (17) yields:

$$\delta\rho^{m+1} = \delta\rho_{int} - \frac{1}{2c^2}\delta p_{int} + \frac{\rho}{2c}(v_l^{m+1} - v_l^m),$$

$$\delta v^{m+1} = v_l^{m+1} - v_l^m, \quad \delta p^{m+1} = \frac{1}{2}[\delta p_{int} + + \rho c(v_l^{m+1} - v_l^m)]. \tag{31–33}$$

5. VALIDATION OF THE MODEL

The numerical model will now be validated in the case of a linear flow regime for which there are analytical solutions. The geometry considered is based on the standard lined duct test case of reference [4]. Depicted in Figure 2, the 2D duct has the following dimensions:

$$L = 0{\cdot}9144 \text{ m}, \quad D = 0{\cdot}1524 \text{ m}, \quad H = 0{\cdot}3048 \text{ m}.$$

The lined part of the top surface is represented via the liner model. Plane pressure waves are imposed at the right-hand side boundary, while the left-hand side boundary is treated as open. All quantities are non-dimensionalized by using the following reference scales: $l_r = 0{\cdot}3048$ m $\rightarrow$ length scale; $u_r = 340{\cdot}25$ m/s $\rightarrow$ velocity scale; $\rho_r = 1{\cdot}225$ kg/m^3 $\rightarrow$ density scale; $l_r/u_r = 8{\cdot}958\,10^{-4}$ s $\rightarrow$ time scale; $\rho_r u_r^2 = 1{\cdot}418\,10^5$ Pa $\rightarrow$ pressure scale. Here standard atmospheric density and speed of sound are used as reference values.

The results will be presented in terms of sound pressure level (SPL) distributions and power transmitted along the duct per span (P/span). The SPL is defined as:

$$SPL = 10 \log_{10} \left[\frac{(\rho_r^2 u_r^4/T) \int_0^T (p(t) - \bar{p})^2 \, \mathrm{d}t}{\tilde{p}_{ref}^2} \right], \tag{34}$$

where T is the period of the wave, $\bar{p}$ is the non-dimensional pressure averaged over T and $\tilde{p}_{ref}$ is the reference root-mean-square (RMS) pressure fluctuation set to 2×10^{-5} Pa.

The axial intensity, due to the perturbation of the energy flux, is defined as

$$I_x = \frac{1}{T} \int_0^T (\rho h u - \overline{\rho h u}) \, \mathrm{d}t \tag{35}$$

while $P/span$ is computed as

$$P/span = \int_{y_{min}}^{y_{max}} I_x \, \mathrm{d}y. \tag{36}$$

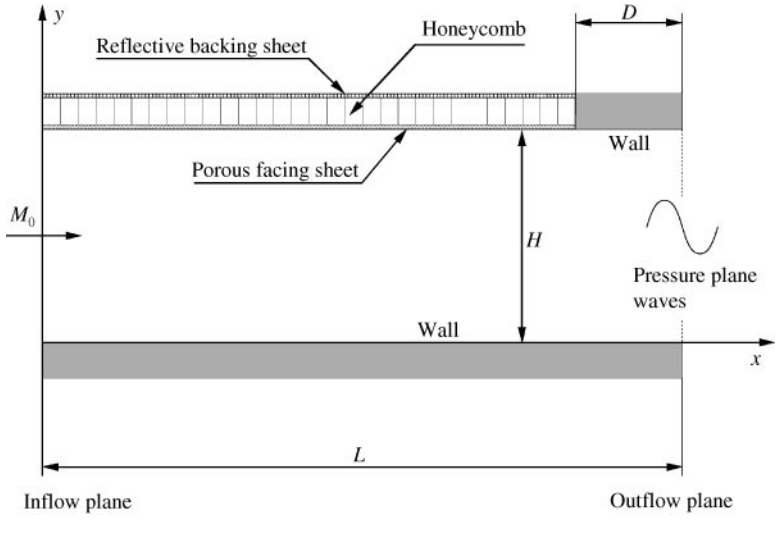

Figure 2. Geometry of the 2D test case.

5.1. PURE-TONE SIGNAL

A pure-tone sinusoidal pressure wave was applied to the outflow plane with a very small amplitude (1% of the average pressure value) and a frequency of 250 Hz. Since the regime is linear, the liner non-dimensional resistance is governed only by the linear term $R_{td} = R_l = 0{\cdot}5$. The cavity depth was set to 0·254 m. This depth has an unrepresentative value as it is designed to give high attenuation at low frequency where only one mode is propagating. In the absence of liners, the pressure waves propagate along the duct with no attenuation, and the *SPL* computed by using relation (34), remains constant at 151 dB.

For such a test case, it is possible to obtain analytical solutions by using linearized single-frequency methods based on linearized inviscid flow equations [10]. Two sets of calculations have been performed and compared with the analytical solutions: the first one is the prediction of the pressure wave decay rate in the case of zero mean flow ($M_0 = 0$) while the second one has a mean flow ($M_0 = 0{\cdot}4$). These two cases test the ability of the liner model to predict the sound decay rates correctly and the ability of the code to allow the waves to exit the open left boundary without any spurious reflections.

5.1.1. *Zero mean flow*

The spatial discretization of the duct domain has been obtained by generating a simple rectangular grid with 120 points in the axial direction and 40 points in the transversal direction (see Figure 3). Remembering that the pressure waves propagate in the duct with the speed of sound and using the reference quantities in (34), one finds the length of a wave with a frequency of 250 Hz to be around 4·5 times the length scale l_r, and thus, 1·5 times the total length of the duct. Following such considerations, the total number of points per axial wave length (PPW) can be determined as 180. The minimum recommended value of 50 PPW suggested in references [13, 14], implies that this level of discretization guarantees virtually zero numerical dissipation. The non-dimensional time step used for the numerical simulation is 0·005; thus it takes nearly 900 time iterations to compute one period of the signal. The numerical solution is considered to be converged when it becomes periodic. Such a state is reached after 4 periods, which means that all calculations need to be performed using about 5000 time steps. Such a calculation takes about 20 min on a 266 MHz PC. Figure (4) shows the *SPL* along the duct for different y-stations. At $y/l_r = 1$, which corresponds to the lined wall, the *SPL* values are higher than at all the other y-stations. On the other hand, the slopes of all the *SPL* curves are nearly the same at about 10 dB per length scale l_r. This is in good agreement with the analytical solution which also predicts an attenuation rate of 10 dB per length scale. Figure (5) shows the power drop per span for standard and long duct-domain simulations. This figure demonstrates that

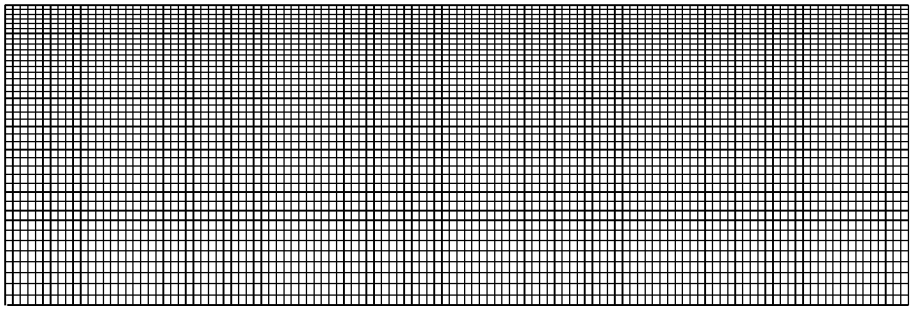

Figure 3. Computational domain for the 2D test case.

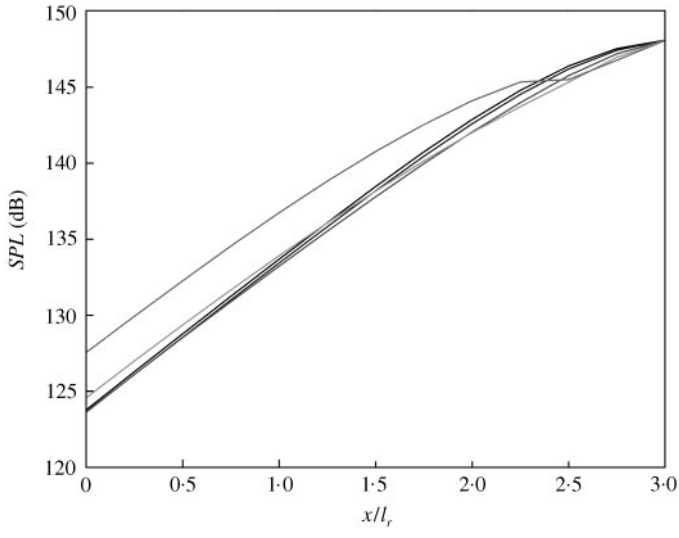

Figure 4. Pure-tone signal: SPL along the duct with zero mean flow. Curves, from left bottom to top: $y/z_r = 0$, 0·287, 0·521, 0·714, 1.

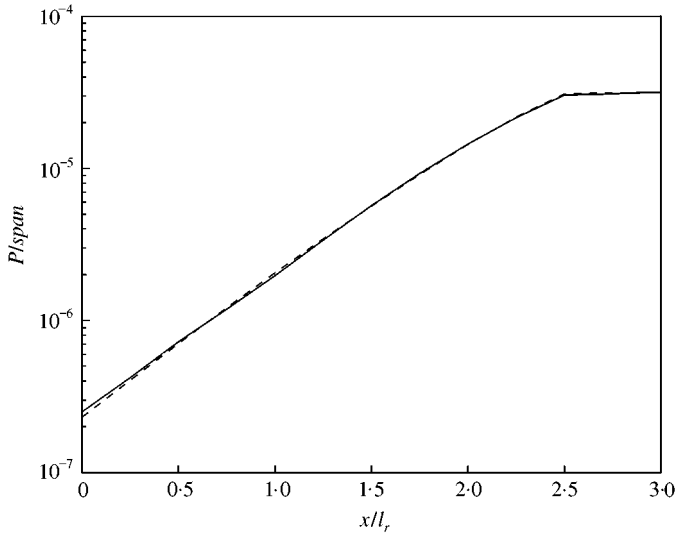

Figure 5. Pure-tone signal: power drop/span with zero mean flow. ——, Short domain; – – –, long domain.

degradation from boundary reflections is small. Figure (6) shows 16 unsteady pressure contour plots for the duct domain during one period of the imposed signal. This figure clearly indicates the absorption of high and low pressures by the upper wall which is treated by the liner model. A kink around $x/l_r = 2{\cdot}5$ is observed in both figures, a feature due to the fact that the liner finishes at that location.

5.1.2. *Subsonic mean flow*

This test case differs from the previous one because of the presence of a subsonic mean flow with a Mach number of 0·4. The behaviour of the liner model changes since the

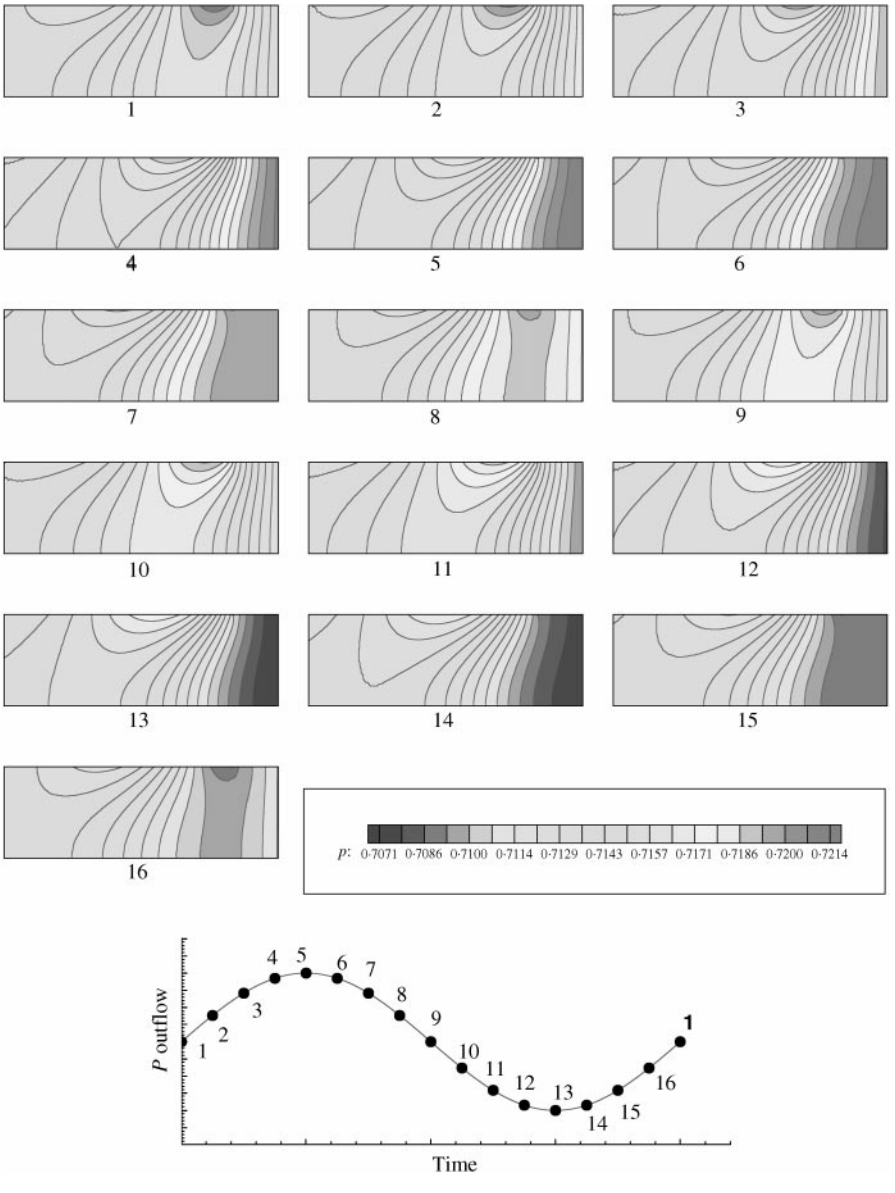

Figure 6. Pure-tone signal: pressure time history with zero mean flow.

presence of any mean flow causes the term $\bar{u}(\partial v/\partial x)$ in equation (15) to become significant. This term represents the jump of the normal velocity across the vortex sheet in the lined wall due to the presence of a boundary layer. Figure (7) shows the *SPL* along the axial direction of the duct for different transversal stations. The slope of all five curves in the $0 \leqslant x/l_r \leqslant 1$ region remains constant at about 7·5 dB per length scale, a prediction which is again in very good agreement with the analytical solution of 7·4 dB.

If one compares the *SPL* along the duct for the cases of zero- and non-zero-mean flows (Figures 4 and 7), one feature is striking: for zero-mean flow, the *SPL* at a given axial co-ordinate is higher in the lined wall but this is no longer true in the case of mean flow. The

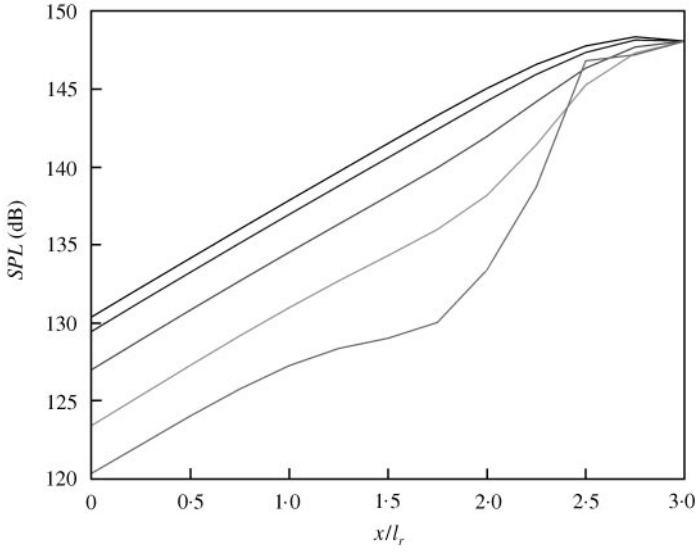

Figure 7. Pure-tone signal: *SPL* along the duct with mean flow. $M_0 = 0{\cdot}4$. Curves, from left, top to bottom: $y/z_r = 0$, 0·287, 0·521, 0·714, 1.

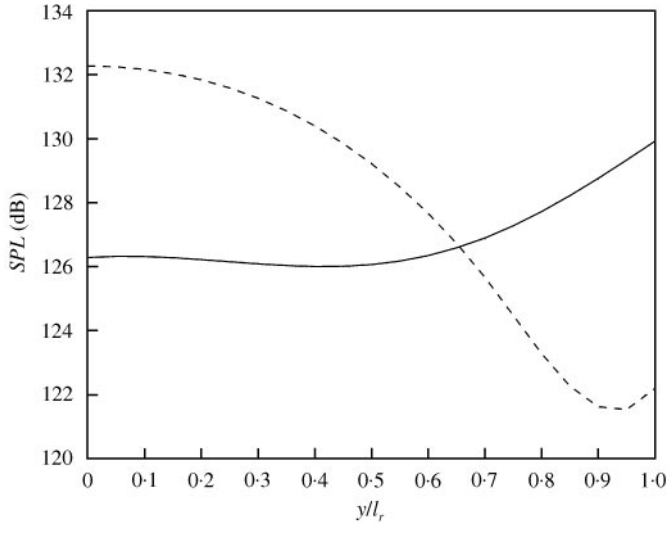

Figure 8. Pure-tone signal: *SPL* along transversal direction. ——, $M_0 = 0$; – – –, M_0 0·4.

same feature is more apparent in Figure 8 where the *SPL* for the two cases are plotted along the y-coordinate at $x/l_r = 0{\cdot}25$.

Figure 9 shows the power drop per span obtained using the standard and extended duct domains. The amount of reflection at the left boundary is higher than that in the case of zero-mean flow (see Figure 5). The reason for such behaviour can be traced back to the numerical evaluation of the derivative in equation (19) for point i at the open boundary. This derivative is evaluated in an upwind manner in order to have a stable scheme and it is set to zero for point i at the left boundary. A better approximation to this derivative should reduce the amount of spurious reflections at the left boundary. The power drop per span is

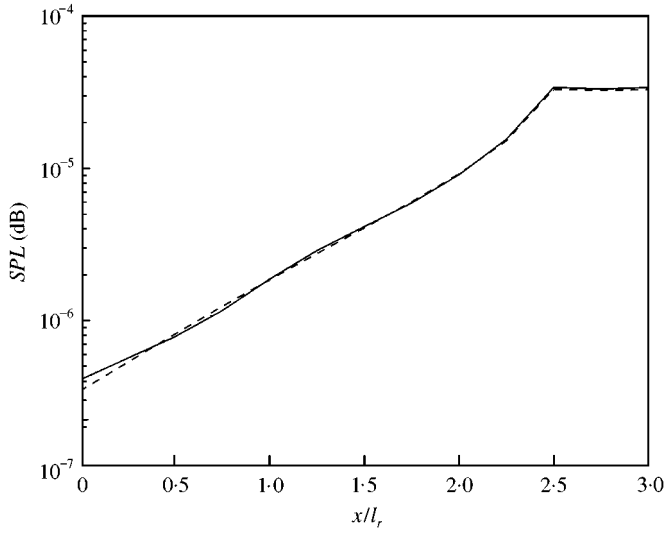

Figure 9. Pure-tone signal: power drop/span. ——, Short domain; – – –, long domain.

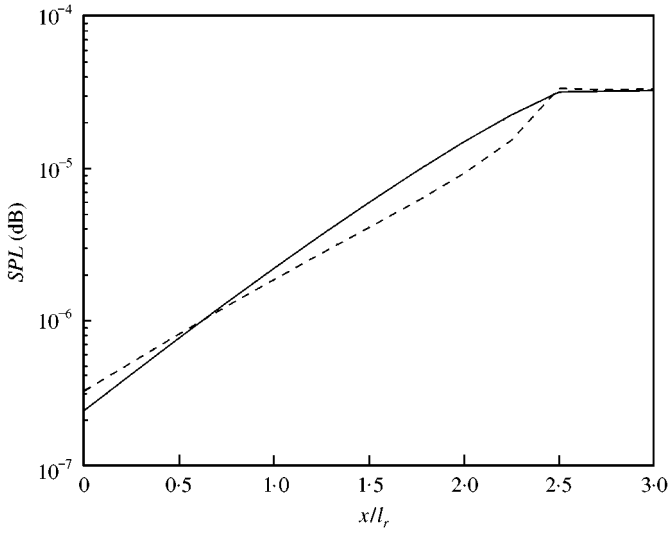

Figure 10. Pure-tone signal: power drop/span zero and non-zero mean flow. ——, $M_0 = 0$; – – –, $M_0 = 0{\cdot}4$.

compared for zero and finite mean flow cases in Figure 10. There is a marked slope difference between the two curves at the inflow portion of the duct.

Figures 11 and 12 show the *RMS* values[†] of pressure and velocity in the liner cavity at $x/l_r = 1{\cdot}5$ (middle of the duct) for Mach numbers of 0 and 0.4. The location $l_c/l_r = 0$ corresponds to the liner porous sheet, while $l_c/l_r = 0{\cdot}833$ corresponds to the reflective backing sheet where the velocity is set to zero.

[†]The *RMS* of a quantity u over the period T is defined by $RMS(u) = \sqrt{(1/T)\int_0^T (u(t) - \bar{u})^2 \, \mathrm{d}t}$.

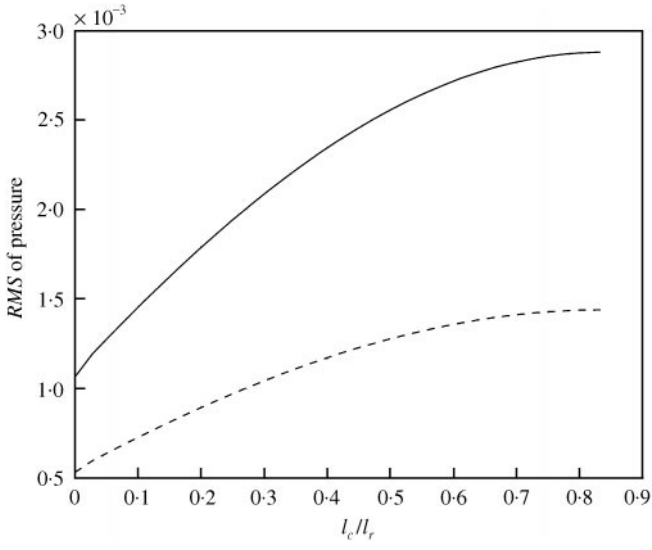

Figure 11. Pure-tone signal: *RMS* of pressure in the liner cavity at the middle of the duct. ——, $M_0 = 0$; – – –, $M_0 = 0{\cdot}4$.

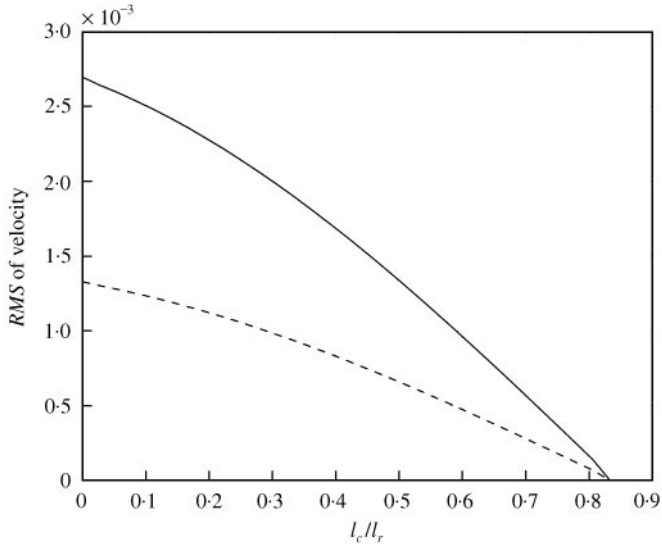

Figure 12. Pure-tone signal: RMS of velocity in the liner cavity at the middle of the duct. ——, $M_0 = 0$; – – –, $M_0 = 0{\cdot}4$.

5.2. LINEAR N-WAVE SIGNAL

The pressure signal imposed at the outflow will now take the form of an *N*-wave but the amplitude and frequency of the pressure wave, the liner resistance and the cavity depth will remain unchanged. The computational grid of the pure-tone case is also used here (see Figure 3). The results for the case of zero mean flow are shown in Figures 13–16. The decay rate of the first harmonic is about 10 dB per length scale l_r which

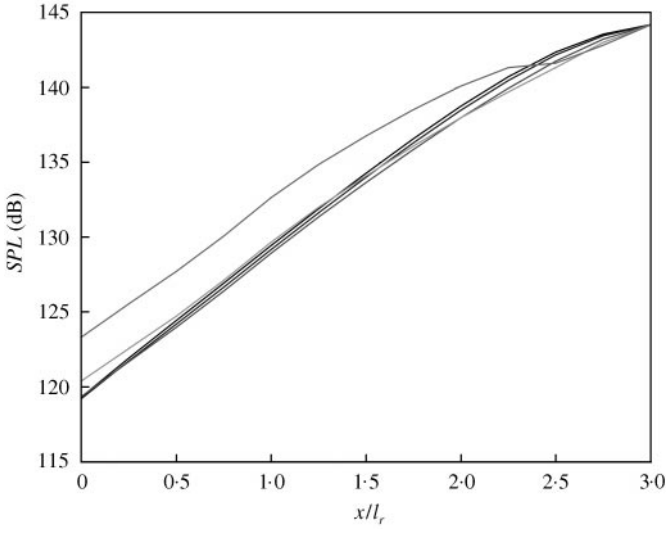

Figure 13. Linear *N*-wave: *SPL* of first harmonic for zero mean flow. Curves, from left, bottom to top: $y/z_r = 0$, 0·287, 0·521, 0·714, 1.

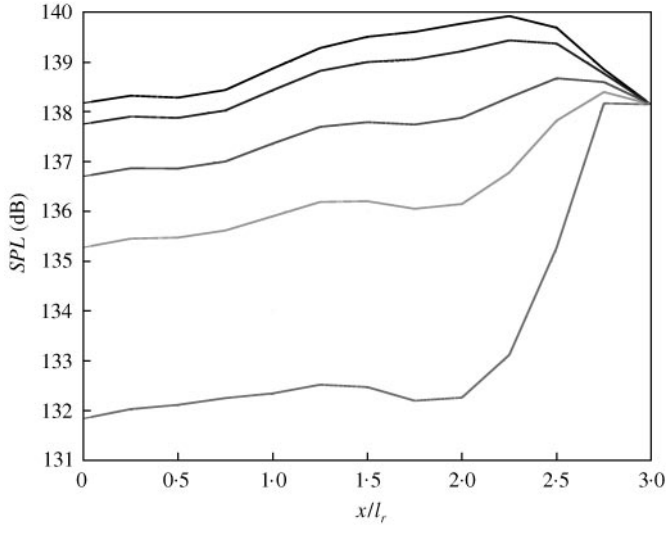

Figure 14. Linear *N*-wave: *SPL* of second harmonic for zero mean flow. Curves, from left, top to bottom: $y/z_r = 0$, 0·287, 0·521, 0·714, 1.

is almost identical to that obtained for the pure-tone signal. The decay rate for the second harmonic is very close to the analytical value of 0·5 db per length scale, while the decay rate for the third harmonic is seen to be different for different *y*-stations. For this particular harmonic, the analytical results indicate a decay rate of 0·13 db per length scale, which is quite different from the numerical predictions. This discrepancy is probably due to the limitation of the liner resistance model which is considered to be frequency independent.

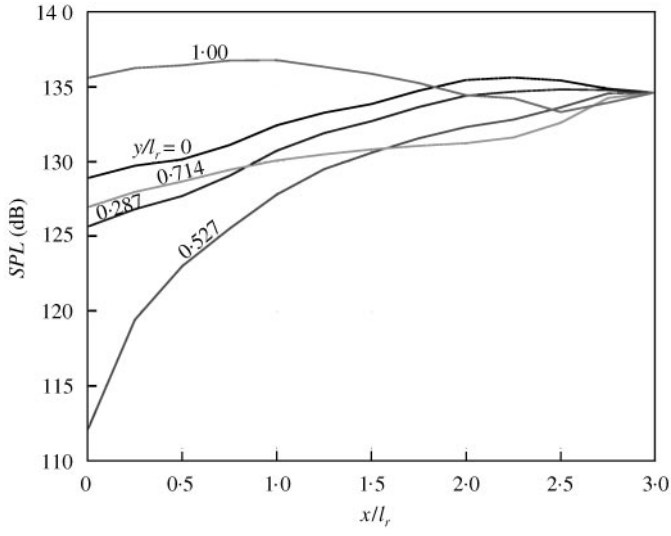

Figure 15. Linear *N*-wave: *SPL* of third harmonic far. Zero mean flow.

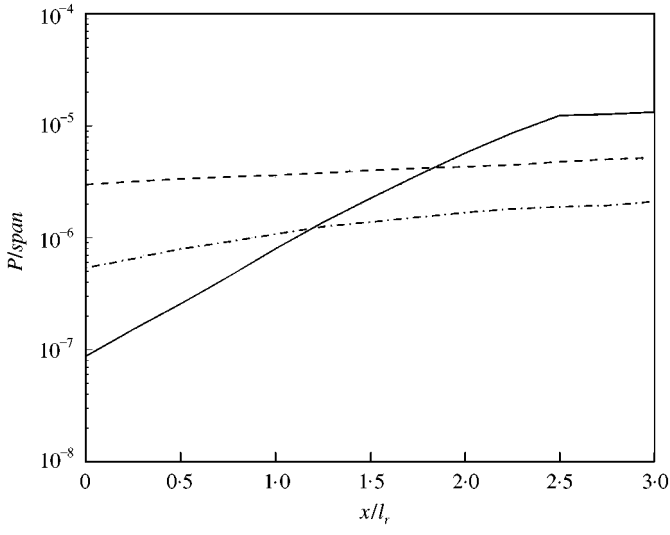

Figure 16. Linear *N*-wave: power drop/span for zero mean flow: ——, 1st harmonic; – – –, 2nd harmonic; – · – · –, 3rd harmonic.

6. CONCLUSIONS AND FURTHER WORK

A time-domain laminar liner model suitable for aero-engines applications has been developed. The model combines a frequency-independent resistive part and a reactive part which is obtained by solving the flow within the liner cavity. The model is valid with and without mean flows, as well as for linear and non-linear sound propagation. The model has been validated for the linear cases by comparing the computational results on a 2D duct with the analytical ones. Good agreement is obtained in all cases considered.

The main features of the model are as follows: (i) Multi-frequency problems can be solved in one calculation. (ii) The frequency dependence of the liner impedance does not appear

explicitly in the formulation of the model but this effect is taken into account in the reactance model through the solution of the flow within the liner cavity. (iii) The liner model is characterized by three parameters only: the linear and non-linear parts of the resistance (R_l and R_{nl}) and the cavity depth d. This is an important feature if one has to perform a parametric study of the liner response.

The method can be used for non-linear sound attenuation in the case of zero-mean flow, even though no numerical results are given for this case. For inviscid, non-zero mean flows, a velocity discontinuity occurs at the liner boundary. Although it is possible to linearize such a jump, a more accurate treatment in principle, is possible by viscous modelling of the main flow. However, such an approach will have to deal with turbulent boundary layers and flow separation from the porous layers.

In the case of a linear N-wave, the decay rates of the first two harmonics were predicted correctly, while that for the third wave differs significantly from the analytical solution. This is probably due to the limitation of the liner resistance formulation which is assumed to be frequency independent, An improved model which includes a frequency-dependent liner resistance will be discussed in a forthcoming paper.

ACKNOWLEDGMENTS

The authors thank Rolls–Royce plc for sponsoring this work and allowing its publication. Many useful discussions with Prof. J. W. Chew of Surrey University, Dr. A. Wilson of Rolls–Royce plc and Dr. M. Fisher of Southampton University are also gratefully acknowledged.

REFERENCES

1. M. K. MYERS 1980 *Journal of Sound and Vibration* **71**, 429–434. On the acoustic boundary conditions in the presence of flow.
2. R. G. WHITE and J. G. WALKER (editors) 1982 *Noise and Vibration*. Chichester: Wiley.
3. Y. ÖZYÖRÜK 1995 *Ph.D. Thesis, Pennsylvania State University*. Sound radiation from ducted fans using computational aeroacoustics on parallel computers.
4. R. S. REICHERT and S. BIRINGEN 1997 *AIAA Paper* 97-1650-*CP*. Time domain simulation of acoustic propagation in a lined duct.
5. R. C. SWANSON and E. TURKEL 1992 *Journal of Computational Physics* **101**, 292–306. On central-difference and upwind schemes.
6. P. C. JORGENSON and E. TURKEL 1993 *Journal of Computational Physics* **107**, 297–308. Central difference TVD schemes for time dependent and steady state problems.
7. C. W. SHU 1988 *SIAM Journal on Scientific and Statistical Computing* **9**, 1073–1084. Total Variation Diminishing Time Discretisations.
8. M. B. GILES 1990 *AIAA Journal* **28**, 2050–2058. Non-reflecting boundary conditions for the Euler equations calculations.
9. T. H. MELLING 1973 *Journal of Sound and Vibration* **29**, 1–65. The acoustic impedance of perforates at medium and high sound pressure levels.
10. B. J. TESTER 1973 *Journal of Sound and Vibration* **28**, 151–203. The propagation and attenuation of sound in lined ducts containing uniform "Plug" Flow.
11. B. J. TESTER 1973 *Journal of Sound and Vibration* **28**, 217–245. Some aspects of sound attenuation in lined ducts containing inviscid mean flows with boundary layers.
12. C. HIRSCH 1990 *Numerical Computation of Internal and External Flows*. Vol. 1–2. New York: Wiley.
13. L. SBARDELLA 1997 *Technical Report VUTC/C/97004 Imperial College, London*. CFD analysis of noise propagation.
14. D. P. LOCKARD, K. S. BRENTNER and H. L. ATKINS 1995 *AIAA Journal* **33**, 246–251. High-accuracy algorithm for computational aeroacoustics.